



An extended carbonyl-rich conjugated polymer cathode for high-capacity lithium-ion batteries†

Cite this: *J. Mater. Chem. A*, 2021, 9, 2700

Shibing Zheng,^a Licheng Miao,^b Tianjiang Sun,^a Lin Li,^a Tao Ma,^a Junquan Bao,^a Zhanliang Tao^{*a} and Jun Chen^a

Received 30th November 2020
Accepted 16th January 2021

DOI: 10.1039/d0ta11648c

rsc.li/materials-a

Organic materials have attracted extensive attention for use in lithium-ion batteries due to the flexible designability of their structures and their high theoretical capacities. However, the high solubilities, low voltages, and poor conductivities of traditional organic materials have impeded their further application. Herein, a novel carbonyl-rich covalent organic polymer (COP), polyphenyl-1,3,5-(pyrene-4,5,9,10-tetraone) (PPh-PTO), was designed and synthesized. *In situ* Fourier-transform infrared spectroscopy (FTIR), *ex situ* X-ray photoelectron spectroscopy (XPS), and Raman analysis were used to confirm the carbonyl redox-active centers. Moreover, density functional theory (DFT) calculations were used to verify that the extended conjugated structure can induce electron delocalization and achieve an elevated and slanted voltage plateau in comparison with the pyrene-4,5,9,10-tetraone (PTO) monomer. The extended structure enables PPh-PTO to show a high reversible capacity of 235 mA h g⁻¹ at 0.1 A g⁻¹, superior cycling abilities (95% capacity retention after 1400 cycles), and excellent rate performance (94 mA h g⁻¹ at 2 A g⁻¹) in lithium-ion batteries. Our work developed a promising strategy for designing high-energy carbonyl-rich covalent organic polymers for energy storage.

Introduction

Eco-friendly and sustainable organic materials are considered as promising substitutes for inorganic materials for use in lithium-ion batteries.^{1,2} Investigations into various materials with different active centers (carbonyls, nitriles, radicals, imine compounds, *etc.*) have been widely performed.^{3,4} Among them, conjugated carbonyl compounds have been intensively studied

owing to their high redox reversibility and capacity *versus* other materials.⁵⁻⁷ Pyrene-4,5,9,10-tetraone (PTO), with four carbonyl active sites and a high theoretical capacity of 408 mA h g⁻¹, has attracted attention as cathode material for use in high-energy-density lithium batteries. However, there are inevitable intrinsic drawbacks, including high dissolubility, low conductivity, and a low redox potential. Traditional strategies, including linear polymerization, grafting, and tuning the molecular polarity, are aimed at suppressing the solubility of materials.⁸ Methods for improving potentials include introducing electron-withdrawing groups and heteroatoms (N, S), which can contribute to an increase in electroconductivity.⁹⁻¹¹ Recently, a reported extended conjugated system bearing all these characteristics may have broken the deadlock. Luo *et al.* prepared an extended π -conjugated system showing high-voltage and insoluble properties.¹² Stoddart's group further confirmed that extended macrocycles can delocalize electrons to homogenize the voltage platform, causing a voltage improvement.¹³ Thus, extended conjugated systems seem to have the potential to pave the way for the application of organic materials.

Covalent organic polymers (COPs), sharing the general characteristic of an extended topological structure, are prominent structural skeletons with high designability,^{14,15} porosity, and stability.¹⁶ Their ease of chemical modification extended their application fields to areas such as proton conduction,¹⁷ catalysis,¹⁸ electrolyte membranes,¹⁹ and gas separation.²⁰ Through introducing rational active sites, COPs can be applied to energy storage. For instance, Wang's group successfully prepared covalent organic framework nanosheets, DAAQ-ECOF, exhibiting an excellent capacity of 104 mA h g⁻¹ at 0.5 A g⁻¹ with 95% capacity retention after 1800 cycles.²¹ Xu *et al.* constructed a conjugated microporous polymer based on an imine group, which delivered a capacity of 147 mA h g⁻¹ at 0.1 A g⁻¹ and high cycling stability.²² However, the reported cathodes were still plagued by low capacities and voltages due to active-monomer insufficiencies. Thus, creating an ideal active monomer is of the essence. Representative studies, such as those constructing

^aKey Laboratory of Advanced Energy Materials Chemistry (Ministry of Education), College of Chemistry, Nankai University, Tianjin 300071, China. E-mail: taozhl@nankai.edu.cn

^bCollege of Physics and Optoelectronic Engineering, Shenzhen University, Shenzhen 518060, China

† Electronic supplementary information (ESI) available. See DOI: 10.1039/d0ta11648c

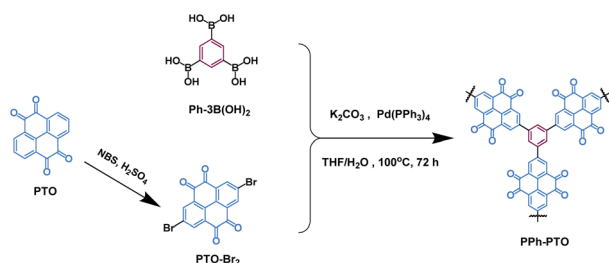
two-dimensional²³ or linear^{24,25} polymers, have achieved excellent performance. Inspired by this, combining the merits of an extended π -conjugated structure with high-energy active sites may be a way to overcome related issues.

Herein, we constructed a novel extended π -conjugated carbonyl-rich covalent organic polymer (PPh-PTO) based on a high-energy monomer (PTO) for lithium-ion batteries. *Ex/in situ* UV-vis and *ex situ* FTIR spectroscopy studies were carried out to verify the insolubility in electrolyte. *In situ* FTIR and *ex situ* XPS studies confirmed that the carbonyl groups were the lithiation/delithiation sites. As predicted, the extended π -conjugation lowered the LUMO level and narrowed the energy gap of PPh-PTO, resulting in voltage and electronic conductivity enhancements. PPh-PTO showed a high capacity of 235 mA h g⁻¹ at 0.1 A g⁻¹, excellent cycling abilities (95% retention after 1400 cycles), and good rate capabilities (95 mA h g⁻¹ at 2 A g⁻¹). Further quantitative kinetic analysis revealed that the discharge/charge process tends to be a redox pseudocapacitive process, which accounts for the fast electrochemical kinetics of PPh-PTO. Our investigation suggests that COP materials based on the rational design of extended conjugated structure can achieve multi-aspect improvement for rechargeable battery applications.

Results and discussion

The PPh-PTO compound was synthesized *via* a Suzuki coupling reaction between the prepared 2,7-dibromo-4,5,9,10-pyrenetetrona (PTO-Br₂) (Fig. S1 and S2†) and 1,3,5-benzene-tribonic acid (Scheme 1). The obtained samples were characterized *via* FTIR (Fig. S3†), solid-state ¹³C nuclear magnetic resonance (NMR) spectroscopy (Fig. S4†), and powder X-ray diffraction (XRD, Fig. S5†). PPh-PTO was a brownish-black powder with irregular micron- or sub-micron-sized particles (Fig. S6†). Energy dispersive spectroscopy (EDS) analysis confirmed the presence and homogenous distribution of C, O, and a small amount of Br in as-synthesized PPh-PTO (Fig. S7†). The thermo-gravimetric analysis (TGA) results show that PPh-PTO was stable below 250 °C (Fig. S8†), indicating the safety of PPh-PTO as an active electrochemical material in rechargeable batteries.

To gain insights into the solubility performance of the monomer (PTO) and PPh-PTO, dissolution experiments were performed. We first collected optical photographs and FTIR spectra of electrolytes after different soaking durations (from



Scheme 1 The synthesis route to PPh-PTO.

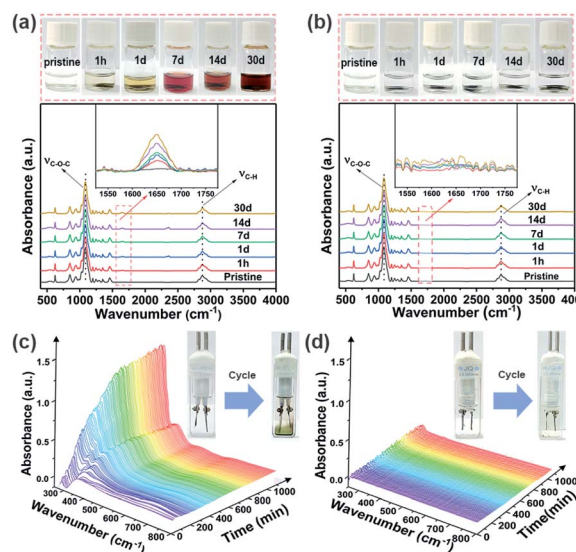


Fig. 1 Optical photographs of (a) PTO and (b) PPh-PTO electrodes in the electrolyte and corresponding FTIR spectra of the electrolyte samples after soaking for different lengths of time. *In situ* UV-vis spectra of electrolyte samples from a (c) Li-PTO battery and (d) Li-PPh-PTO battery (125 mA g⁻¹, collection frequency: every 5 min).

1 h to 1 month). A distinct colour change and corresponding peak increase at 1655 cm⁻¹ (the C=O functional group of PTO) can be observed with an increase in time, while the peaks at 1080 cm⁻¹ (C–O–C stretching vibrations) and 2880 cm⁻¹ (C–H stretching) pertaining to the tetraethylene glycol dimethyl ether (G4) electrolyte remain unchanged (Fig. 1a). Furthermore, an increase in the intensity of the peak at 310 nm can be observed from the UV-vis spectroscopy analysis of PTO (Fig. S9a†). In contrast, the colour and spectra of PPh-PTO solutions remained unchanged (Fig. 1b and S9b†). Also, the morphologies of pristine and soaked (7, 14, and 30 days) PPh-PTO electrodes are very similar (Fig. S10†), indicating the stability of PPh-PTO in the electrolyte. Moreover, *in situ* UV-vis spectroscopy technology was used to compare the dissolution of active materials during the electrochemical reaction in G4. For the PTO battery, an ultraviolet absorption peak from PTO appeared at 310 nm, and this increased with the length of the discharging/charging process (Fig. 1c). However, for the PPh-PTO battery no absorption peak emerged, and the electrolyte remained clear after cycling, suggesting that PPh-PTO is indeed insoluble in the electrolyte (Fig. 1d).

Subsequently, the electrochemical activity of the PPh-PTO electrode was investigated. *In situ*-analysis-suitable and normal CR2032 coin-type cells were assembled and tested at room temperature. *In situ* FTIR was applied to monitor the lithium storage mechanism of PPh-PTO during the discharging/charging process. First, to avoid interference peaks originating from the organic or inorganic matrix at the electrode/electrolyte interface, the spectra of the blank electrode, electrolyte, and PPh-PTO electrode were compared (Fig. S11†). Then we selected a collection section (1690–1660 cm⁻¹) to detect the change in the carbonyl characteristic peak. The discharging and charging

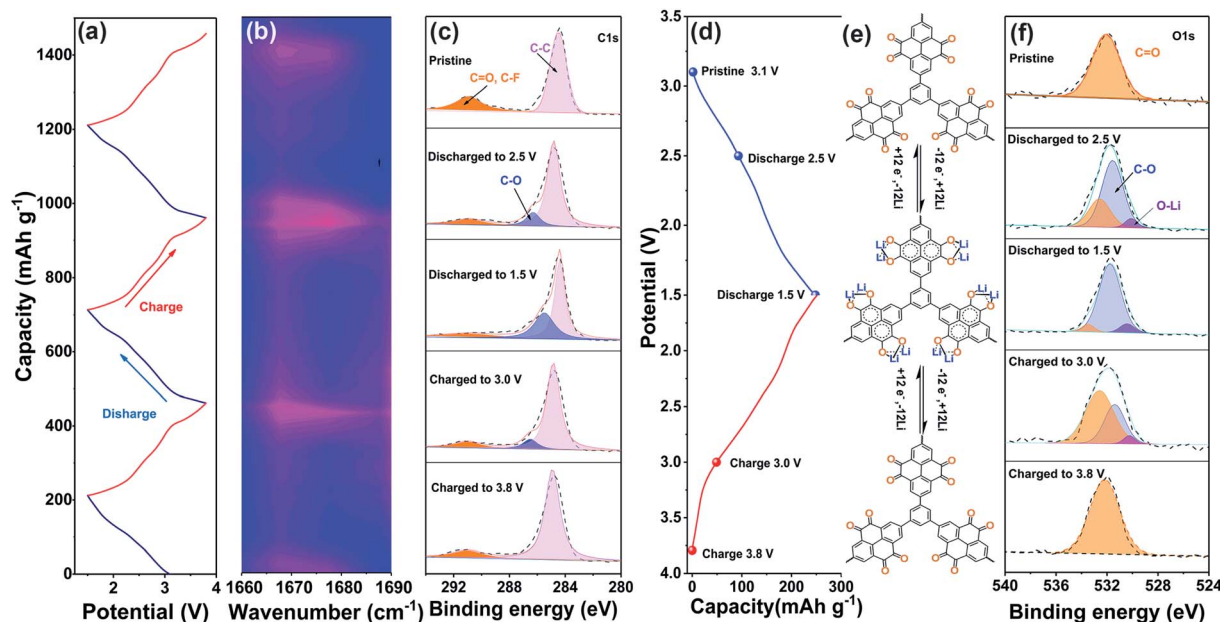


Fig. 2 (a) Discharge and charge curves of PPh-PTO during the first three cycles and (b) the corresponding *in situ* FTIR spectra. High-resolution C 1s (c) and O 1s (f) XPS spectra of pristine PPh-PTO and (d) the corresponding discharge/charge states of the PPh-PTO electrode when discharged to 2.5 V and 1.5 V and charged to 3.0 V and 3.8 V at a current density of 100 mA g⁻¹. (e) The lithiation/delithiation mechanism of PPh-PTO.

curves of PPh-PTO for the first three cycles (Fig. 2a) and the corresponding FTIR spectrum (Fig. 2b) were investigated in real-time. As shown in the colour-map profiles, a reduction in the intensity of the FTIR absorbance peak at around 1670 cm⁻¹ was observed, which corresponded with the carbonyl peak reduction, during the discharge process. Meanwhile, the increase in the intensity of the carbonyl characteristic peak during the charging process was inverse to the decrease during the discharge process, which means that carbonyl oxygen atoms were the active sites of the PPh-PTO electrode.

Moreover, *ex situ* XPS analysis was carried out to further investigate the lithiation/delithiation process during electrochemical cycling. Different discharge/charge states of PPh-PTO electrodes including discharged to 2.5 V and 1.5 V and charged to 3.0 V and 3.8 V at a current density of 100 mA g⁻¹, were measured (Fig. 2d). The XPS spectra of as-prepared PPh-PTO showed two distinct peaks at 284.6 and 531.7 eV in the C 1s and O 1s spectra (Fig. 2c and f), respectively. The C 1s spectrum can be divided into three peaks, located at 284.29, 286.28, and 289.68 eV, which represent sp²-hybridized C-C, C-O, and C=O bonds, respectively (Fig. 2c). The C=O peak (289.68 eV) is weakened during discharging to 2.5 V, and it nearly disappears upon discharging to 1.5 V. Conversely, the C-O peak (286.28 eV) emerged and was enhanced during the discharge process, which can be attributed to the evolution of C=O to C-O-Li as a result of Li⁺ insertion. It is worth noting that the C-O binding peak shifted to a lower binding energy upon discharging from 2.5 to 1.5 V, and it returned to its initial position upon charging to 3.0 V. This phenomenon may be ascribed to the synergistic effect of the adjacent carbonyl. Simultaneously, the changes in the O 1s spectrum peaks at 531.1 eV, 531.76 eV, and 532.42 eV (Fig. 2f), corresponding to O-Li, C-O, and C=O, respectively,

further confirmed the reversibility of the lithiation/delithiation process at the carbonyl active sites (Fig. 2e). Moreover, *ex situ* Raman analysis was conducted to investigate the cathode in different discharge/charge states, which further verified the reversible switch between C=O and C-O during the electrochemical reaction of the PPh-PTO electrode (Fig. S12†).

Compatibility between an electrolyte and electrode material is important. Thus, we first investigated the compatibility between the PPh-PTO electrode and both a popular electrolyte (1 M LiTFSI in DOL/DME (v/v: 1/1)) and the selected electrolyte (1 M LiClO₄/G4). PPh-PTO showed a sharp decay from dissolution and greater polarization in the popular electrolyte than in the 1 M LiClO₄/G4 system (Fig. S13†). Therefore, the further electrochemical testing of PTO and PPh-PTO was carried out in 1 M LiClO₄/G4. Both PTO and PPh-PTO displayed similar cyclic voltammogram (CV) curves, indicating their consistent two-step

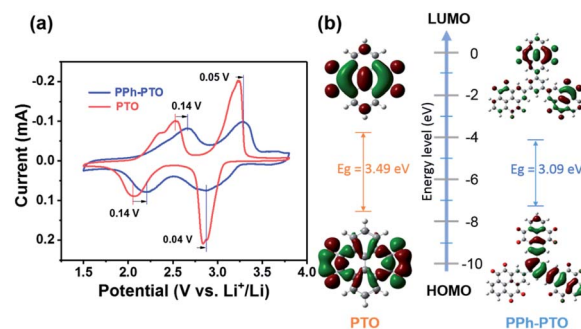


Fig. 3 (a) CV curves of PTO and PPh-PTO at a scan rate of 0.3 mV s⁻¹. (b) The HOMO/LUMO energy levels and orbital plots; E_g is the HOMO-LUMO gap.

lithiation/delithiation processes.²⁶ The PPh-PTO electrode showed two obvious pairs of redox peaks at 2.87/2.18 V for reduction and at 3.28/2.66 V for oxidation at 0.3 mV s⁻¹ (Fig. 3a). As predicted, PPh-PTO has a higher redox potential than PTO due to the extended π -conjugated structure. To verify this, density functional theory (DFT) calculations were performed. PPh-PTO shows a lower LUMO (lowest unoccupied molecular orbital) level (-4.04 eV) compared with that of the PTO monomer (-3.94 eV) (Fig. 3b). For molecules that are closely related in structure, reduction potentials are negatively correlated in a linear fashion with the LUMO energy.²⁷ Therefore, PPh-PTO can achieve a higher reduction potential due to its better electron affinity. Besides, the more extended π -conjugated skeleton of PPh-PTO compared with PTO could induce electron delocalization (see the aromaticity calculations, which included LOL- π (localized orbital locator- π)^{28,29} and HOMA (harmonic oscillator measure of aromaticity)³⁰ calculations, in Fig. S14[†]),

and it therefore exhibited a slanted and elevated voltage plateau. Furthermore, the HOMO-LUMO gap of PPh-PTO (3.09 eV) was narrower than that of PTO (3.49 eV), indicating that the electronic conduction of PPh-PTO will be better.

The galvanostatic discharge-charge profile of PPh-PTO showed an inclined voltage profile due to the delocalization of electrons and it could deliver a high reversible capacity of 220 mA h g⁻¹ (at 0.1 A g⁻¹ and 0.4C) after 1000 cycles (Fig. S13[†]), being more stable than PTO (Fig. S15[†]). The rate performance of the PPh-PTO electrode was estimated at various current densities. As the current density was gradually increased from 20 to 100 to 1000 to 2000 mA g⁻¹, it delivered superior rate capabilities of 243, 224, 191, and 95 mA h g⁻¹, respectively. When the current density was returned to 20 mA g⁻¹, the PPh-PTO electrode recovered a reversible capacity of 244.5 mA h g⁻¹ (Fig. 4a). The sharp decrease in the capacity upon increasing the current from 1000 to 2000 mA g⁻¹ was ascribed to the viscosity of G4.^{26,31}

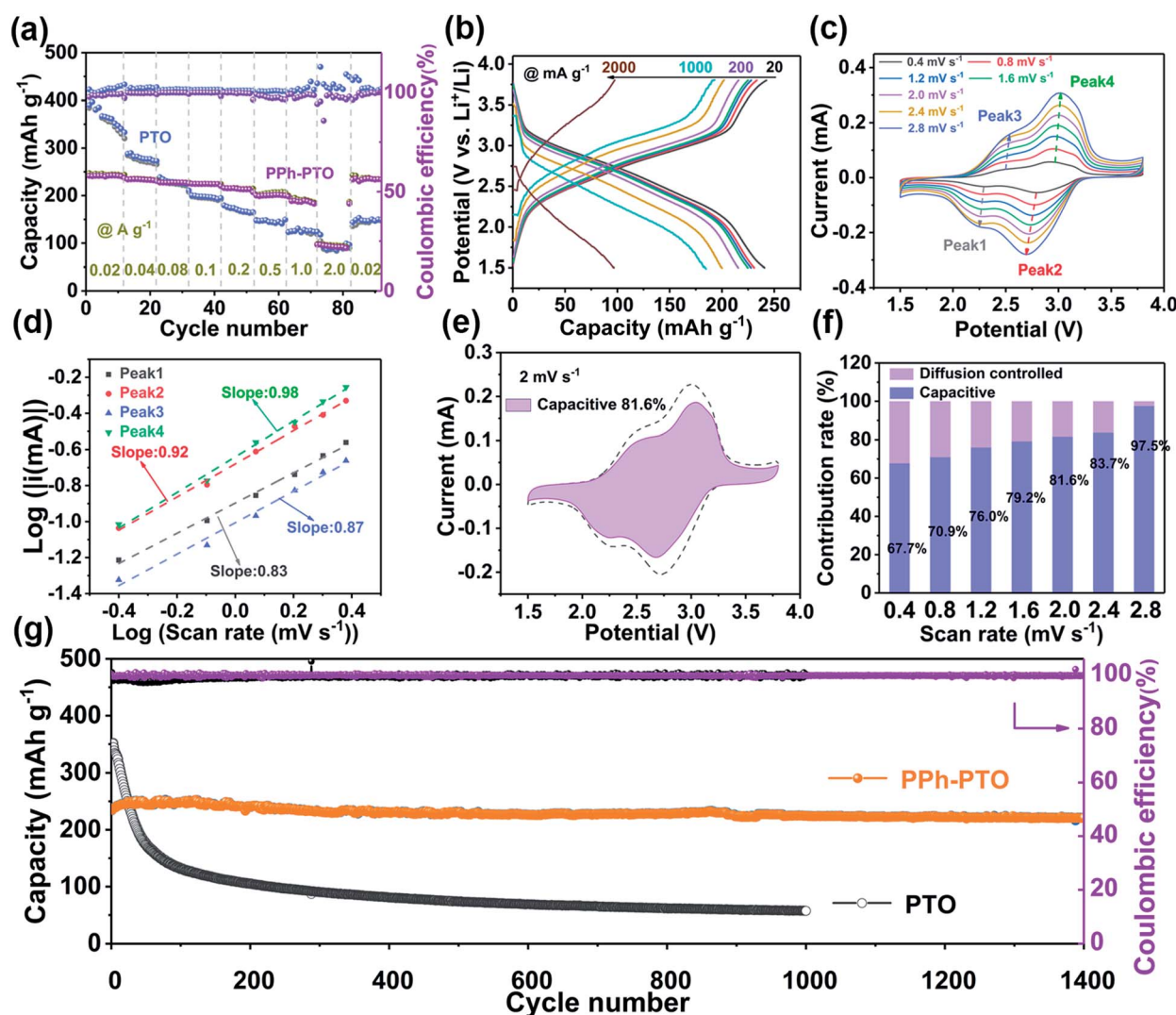


Fig. 4 Quantitative analysis of the charge storage behavior. (a) The rate performances of PTO and PPh-PTO. (b) Discharge and charge profiles of PPh-PTO at different current rates. (c) CV curves from a PPh-PTO electrode at different scan rates from 0.4–2.8 mV s⁻¹ and (d) the relationship between log i and log v . (e) Capacitive and diffusion-controlled contributions at a scan rate of 2 mV s⁻¹. (f) The pseudocapacitive and diffusion-controlled charge storage contributions at different scan rates. (g) The long-term cycling performances of PPh-PTO and PTO at 0.1 A g⁻¹ (0.4C).

However, the PTO monomer with poor electronic conduction delivered inferior rate performance to the polymer, although it showed a high initial capacity. This superior rate performance of PPh-PTO can also be attributed to the specific surface area of the annealed PPh-PTO ($39.99 \text{ m}^2 \text{ g}^{-1}$) and its wide pore-size distribution, which provides sufficient reaction space and ion migration paths after the annealing treatment (Fig. S16†). In addition, the good wettability of $\text{LiClO}_4/\text{G4}$ on the electrode provided another reason for the excellent rate capabilities compared with the PTO monomer (Fig. S17†). Only slight polarization can be observed with an increase in the current for the extended conjugated material (Fig. 4b). The high reversible capacity and coulombic efficiency signified the excellent extended structural and electrochemical stability of PPh-PTO.

To further elucidate the electrochemical kinetics of the PPh-PTO electrode, cyclic voltammetry (CV) measurements were conducted. The CV curves were almost identical upon increasing the sweep rate ($0.4\text{--}2.8 \text{ mV s}^{-1}$), except for slight shifts in the cathodic and anodic peaks (Fig. 4c). Theoretically, the peaks can be divided into capacitive and diffusion components starting from the equation:

$$i = av^b$$

where i is the peak current, v is the scan rate, and a and b are parameters. The b value is the slope of the linear fit of a $\log(v)$ vs. $\log(i)$ plot (Fig. 4d). The cathodic and anodic slope values were calculated to be $0.87/0.98$ and $0.83/0.92$, respectively, indicating that the charge storage mechanism was mainly controlled by capacitive processes. Furthermore, the contribution of the capacitive component at a specific scan rate was calculated according to the equation:

$$i = k_1v + k_2v^{1/2}$$

where k_1v corresponds to the pseudocapacitive contribution and $k_2v^{1/2}$ represents the diffusion-controlled contribution. For instance, the capacitive contribution to the total capacity is 81.6% at a scan rate of 2 mV s^{-1} (Fig. 4e). Furthermore, the pseudocapacitive contribution distribution was summarized. The pseudocapacitive contribution ratio increased manifestly from 67.7% to 97.5% with an increase in the scan rate, revealing that the fast pseudocapacitive behavior accelerates the fast lithiation/delithiation process at high rates and stabilizes the cycling performance (Fig. 4f). Finally, we compared the long-term cycling performance of PPh-PTO with the PTO monomer. PPh-PTO delivered a capacity of 220 mA h g^{-1} after 1400 cycles and retained a high coulombic efficiency of around 100% (Fig. 4g). In comparison, the monomer was highly soluble in the electrolyte, leading to acute capacity decay.

Conclusions

In conclusion, a carbonyl-rich covalent organic polymer, PPh-PTO, was synthesized, and the solubility of organic monomer electrodes was addressed. Extending the conjugated skeleton can delocalize the electronic distribution and narrow the

HOMO–LUMO gap. Thus, carbonyl-rich PPh-PTO delivered a high reduction potential, excellent rate performance (94 mA h g^{-1} at 2 A g^{-1}), and a stable cycling capacity of 224 mA h g^{-1} (0.1 A g^{-1}), with 95% capacity retention after 1400 cycles. Moreover, profiting from its conjugated character, PPh-PTO manifested dominant pseudocapacitive behavior. Quantitative kinetic analysis verified that the pseudocapacitive redox behavior facilitates electrochemical reactions. This work could inspire the design and application of extended π -conjugated COPs for use in high-energy and high-power lithium-ion batteries.

Conflicts of interest

There are no conflicts to declare.

Acknowledgements

This study was supported by the National Key R&D Program of China (2016YFB0901500), National Natural Science Foundation of China (51771094 and 21835004), Ministry of Education of China (B12015 and IRT13R30), and Tianjin Natural Science Foundation (No. 18JCZDJC31500).

Notes and references

- P. Poizot, J. Gaubicher, S. Renault, L. Dubois, Y. Liang and Y. Yao, *Chem. Rev.*, 2020, **120**, 6490–6557.
- Y. Lu and J. Chen, *Nat. Rev. Chem.*, 2020, **4**, 127–142.
- Y. Liang, Z. Tao and J. Chen, *Adv. Energy Mater.*, 2012, **2**, 742–769.
- Z. Song and H. Zhou, *Energy Environ. Sci.*, 2013, **6**, 2280–2301.
- H. Wang, C. Yao, H. Nie, K. Wang, Y. Zhong, P. Chen, S. Mei and Q. Zhang, *J. Mater. Chem. A*, 2020, **8**, 11906–11922.
- M. Bhosale, S. Chae, J. Kim and J. Choi, *J. Mater. Chem. A*, 2018, **6**, 19885–19911.
- M. Yao, H. Senoh, S. Yamazaki, Z. Siroma, T. Sakai and K. Yasuda, *J. Power Sources*, 2010, **195**, 8336–8340.
- D. Heard and A. Lennox, *Angew. Chem., Int. Ed.*, 2020, **59**, 18866–18884.
- Y. Zhang, J. Wang and S. Riduan, *J. Mater. Chem. A*, 2016, **4**, 14902–14914.
- Y. Chen and C. Wang, *Acc. Chem. Res.*, 2020, **53**, 2636–2647.
- X. Yin, S. Sarkar, S. Shi, Q. Huang, H. Zhao, L. Yan, Y. Zhao and J. Zhang, *Adv. Funct. Mater.*, 2020, **30**, 1908445.
- Z. Luo, L. Liu, Q. Zhao, F. Li and J. Chen, *Angew. Chem., Int. Ed.*, 2017, **56**, 12561–12565.
- D. Kim, K. Hermann, A. Prokofjevs, M. T. Otley, C. Pezzato, M. Owczarek and J. F. Stoddart, *J. Am. Chem. Soc.*, 2017, **139**, 6635–6643.
- Y. Zhi, Z. Wang, H. Zhang and Q. Zhang, *Small*, 2020, **16**, 2001070.
- T. Sun, J. Xie, W. Guo, D. Li and Q. Zhang, *Adv. Energy Mater.*, 2020, **10**, 1904199.
- D. Jiang, *Chem*, 2020, **6**, 2461–2483.
- H. Xu, S. Tao and D. Jiang, *Nat. Mater.*, 2016, **15**, 722–726.

- 18 P. Peng, Z. Zhou, J. Guo and Z. Xiang, *ACS Energy Lett.*, 2017, **2**, 1308–1314.
- 19 Y. Hu, N. Dunlap, S. Wan, S. Lu, S. Huang, I. Sellinger, M. Ortiz, Y. Jin, S. H. Lee and W. Zhang, *J. Am. Chem. Soc.*, 2019, **141**, 7518–7525.
- 20 Z. Wang, S. Zhang, Y. Chen, Z. Zhang and S. Ma, *Chem. Soc. Rev.*, 2020, **49**, 708–735.
- 21 S. Wang, Q. Wang, P. Shao, Y. Han, X. Gao, L. Ma, S. Yuan, X. Ma, J. Zhou, X. Feng and B. Wang, *J. Am. Chem. Soc.*, 2017, **139**, 4258–4261.
- 22 F. Xu, X. Chen, Z. Tang, D. Wu, R. Fu and D. Jiang, *Chem. Commun.*, 2014, **50**, 4788–4790.
- 23 C. Yao, Z. Wu, J. Xie, F. Yu, W. Guo, Z. Xu, D. Li, S. Zhang and Q. Zhang, *ChemSusChem*, 2020, **13**, 2457–2463.
- 24 J. Xie, Z. Wang, Z. Xu and Q. Zhang, *Adv. Energy Mater.*, 2018, **8**, 1703509.
- 25 J. Xie, W. Chen, G. Long, W. Gao, Z. Xu, M. Liu and Q. Zhang, *J. Mater. Chem. A*, 2018, **6**, 12985–12991.
- 26 T. Nokami, T. Matsuo, Y. Inatomi, N. Hojo, T. Tsukagoshi, H. Yoshizawa, A. Shimizu, H. Kuramoto, K. Komae, H. Tsuyama and J. Yoshida, *J. Am. Chem. Soc.*, 2012, **134**, 19694–19700.
- 27 Y. Liang, P. Zhang and J. Chen, *Chem. Sci.*, 2013, **4**, 1330–1337.
- 28 H. Schmider and A. Becke, *J. Mol. Struct.*, 2000, **527**, 51–56.
- 29 S. Steinmann, Y. Mo and C. Corminboeuf, *Phys. Chem. Chem. Phys.*, 2011, **13**, 20584–20592.
- 30 L. Miao, L. Liu, K. Zhang and J. Chen, *ChemSusChem*, 2020, **13**, 2337–2344.
- 31 K. Yoshida, M. Nakamura, Y. Kazue, N. Tachikawa, S. Tsuzuki, S. Seki, K. Dokko and M. Watanabe, *J. Am. Chem. Soc.*, 2011, **133**, 13121–13129.